

Radio–optical reference frame link using the US Naval Observatory astrograph and deep CCD imaging

N. Zacharias^{1,3}, M.I. Zacharias^{2,3}

`nz@usno.navy.mil`

¹*U.S. Naval Observatory, 3450 Mass.Ave. NW Washington, DC 20392;*

²*U.S. Naval Observatory (contractor);*

³*Visiting astronomer, Cerro Tololo Inter-American Observatory and Kitt Peak National Observatory, National Optical Astronomy Observatories, which are operated by the Association of Universities for Research in Astronomy, under contract with the National Science Foundation.*

ABSTRACT

Between 1997 and 2004 several observing runs were conducted mainly with the CTIO 0.9 m to image ICRF counterparts (mostly QSOs) in order to determine accurate optical positions. Contemporary to these deep CCD images the same fields were observed with the US Naval Observatory (USNO) astrograph in the same bandpass. They provide accurate positions on the Hipparcos/Tycho-2 system for stars in the 10 to 16 magnitude range used as reference stars for the deep CCD imaging data. Here we present final optical position results of 413 sources based on reference stars obtained by dedicated astrograph observations which were reduced following 2 different procedures. These optical positions are compared to radio VLBI positions. The current optical system is not perfectly aligned to the ICRF radio system with rigid body rotation angles of 3 to 5 mas ($= 3 \sigma$ level) found between them for all 3 axes. Furthermore, statistically, the optical–radio position differences are found to exceed the total, combined, known errors in the observations. Systematic errors in the optical reference star positions as well as physical offsets between the centers of optical and radio emissions are both identified as likely causes. A detrimental, astrophysical, random noise (DARN) component is postulated to be on about the 10 mas level. If confirmed by future observations, this could severely limit the Gaia to ICRF reference frame alignment accuracy to an error of about 0.5 mas per coordinate axis with the current number of sources envisioned to provide the link. A list of 36 ICRF sources without the detection of an optical counterpart to a limiting magnitude of about $R=22$ is provided as well.

Subject headings: astrometry — reference systems — catalogs — quasars:general — galaxies:structure

1. Introduction

The Hipparcos Catalogue (ESA 1997) is currently the primary optical reference frame. It is linked to the defining radio International Celestial Reference Frame (ICRF) by various methods with a dozen radio stars observed with Very Long Baseline Interferometry (VLBI) having the greatest weight (Kovalevsky et al. 1997). An improved version of the ICRF, the ICRF2 (Fey et al. 2009) now contains over 3400 compact, extragalactic sources on the same coordinate system, which is

assumed to be inertial.

The Hipparcos Celestial Reference frame (HCRF) is entirely based on space mission observations and contains positions, proper motions and parallaxes of over 100,000 bright stars on the milli-arcsecond (mas) level (mas/yr for individual proper motions). Zonal and magnitude dependent errors in the Hipparcos Catalogue are estimated to be even smaller. The HCRF is estimated to be accurate to 0.6 mas (1σ) in its alignment to the ICRF at the epoch of 1991.25 with an estimated 0.25 mas/yr (1σ) residual system rotation error

per rigid body angle as compared to the ICRF (Kovalevsky et al. 1997).

The Tycho-2 catalog is the first step of the densification of the optical reference frame to contain the 2.5 million brightest stars to visual magnitude about 11 (Høg et al. 2000). Random position errors of Tycho-2 stars are about 7 mas per coordinate at $V = 9$ and epoch 1991, increasing for the fainter stars. The random error of Tycho-2 star proper motions is typically about 2 mas/yr. The Tycho-2 data are based on Hipparcos star tracker observations (at mean epoch of 1991.25) combined with over 140 ground-based star catalogs to provide sufficient leverage in epoch difference for precise proper motions. The largest weight of the early epoch data in Tycho-2 comes from the Astrographic Catalogue (AC) (Urban et al. 1998), with positions of photographic plates at an epoch around 1900. The AC plates cover an area of just over 2° by 2° and Hipparcos stars were used for their astrometric reductions. Although great care has been taken in these reductions, remaining systematic errors on the AC plates are estimated to be on the 100 mas level, maybe more (Urban, private com.). This results in possible systematic errors of Tycho-2 proper motions on the 1 to 2 mas/yr level.

The goal of this paper is to examine the link between the defining radio reference frame (ICRF) and the optical reference frame (HCRF) by observing the optical counterparts of ICRF sources on the HCRF using the Tycho-2 as reference star catalog in a 2-step process to bridge the large magnitude difference. While the deep CCD imaging captures the optical counterparts, the USNO astrograph is used to provide intermediate bright (12 to 16 mag) reference stars.

Besides possible systematic errors in the optical reference frame (i.e. Tycho-2) the assumption of coinciding centroids of the radio and optical centers of emissions of the extragalactic sources is questioned. Observed optical–radio position offsets are found to be larger than expected from the combination of all known, random errors. Clues for both cases, reference frame issues, and physical offset between radio and optical centers of emission are found. If the later turns out to be a wide-spread issue on the several mas level this would have serious consequences for the alignment accuracy of the future optical, celestial reference

frame from the Gaia mission (Taris et al. 2013) to the ICRF. Our data are not precise enough to make that case; however, some individual sources are found with relatively large radio-optical position offsets likely on the 30 mas level, a few with even much larger offsets, indicating a physical non-coincidence of the radio-optical centroids.

A possible physical offset between the radio and optical centroid of ICRF sources was first discussed in connection with a correlation to the radio structure index (da Silva Neto 2002). Results from a similar, extensive investigation of 300 optical counterparts were recently published by the Rio de Janeiro group (Assafin et al. 2013). Direct differences between ICRF2 radio positions and optical counterpart positions found in the Sloan Digital Sky Survey (SDSS) DR9 were studied for 1297 common sources in another recent paper (Orosz & Frey 2013). Positions of 22 ICRF sources observed with the SOAR 4.2m and ESO 2.2m telescopes again show a correlation of optical–radio position offsets with radio structure index (Camargo et al. 2012).

Our research presented here is the largest and most accurate such sample published so far related to the original ICRF sources and can be considered as a follow-up to an earlier work based on photographic plates for secondary reference stars (Zacharias et al. 1999). Preliminary results of a subset of these data in collaboration with another group was published earlier (Assafin et al. 2003). The high precision of our current investigation could be achieved by using dedicated astrometric observations along with contemporaneous astrograph observations, thus eliminating the degrading effect of proper motion errors of intermediate bright link stars. Partial, preliminary results of our research were presented at several meetings, (Zacharias 2004), (3), (Zacharias & Zacharias 2005), (Zacharias & Zacharias 2008), (Zacharias & Zacharias 2009) and (4). It was not until recently that the final (4th) USNO CCD Astrograph Catalog (UCAC4) was published (Zacharias et al. 2013) and its reduction process could be adopted for the critical astrograph data to finally conclude with this paper a research program that lasted more than a decade.

2. Observations

Optical positions of ICRF counterparts were derived from a 2-step observing process using the USNO astrograph and the CTIO 0.9 m telescope, respectively. For each 0.9 m run the same fields were observed with the astrograph within about a month. Thus hard-to-come-by accurate proper motions of anonymous medium bright stars common to both sets of observations are not needed excluding a major source of error for the derived optical positions of the ICRF counterparts. The large number of high quality secondary reference stars provided by these astrograph observations also allowed calibration of the 0.9 m data for field angle distortions on the mas level.

For most observing runs both telescopes were located at the same site (Cerro Tololo) and the same bandpass (579 to 643 nm) was used with custom filters. This approach minimizes astrometric errors from differential color refraction (DCR) of the anonymous reference stars common to both data sets. The relatively narrow bandpass also minimizes DCR between the ICRF target source and the set of reference stars.

For a total of 413 sources, mainly in the southern hemisphere, optical positions could be derived. These include AGN, BL-Lac and QSO sources. No photometric observations were performed here. The distribution of redshift as a function of approximate optical magnitude is presented in Fig. 1 with data taken from the LQAC-2 catalog (Souhay et al. 2012).

2.1. CTIO 0.9 m

Table 1 gives a summary of the deep imaging observing runs used for this investigation. All except one made use of the CTIO 0.9 m telescope with its standard 2k by 2k CCD and a scale of 0.4 arcsec/pixel. For a single observing run we used the 2.1m KPNO telescope with its 2k by 2k CCD and 0.3 arcsec/pixel image scale. The last deep observing run “J” (CTIO 0.9 m) was performed a few years after most of the other runs to acquire data on ICRF targets which were missed before or could use more observing. Typically about 4 deep exposures were taken per source and observing run with several arcsec offsets applied between exposures to sample the field of view with different parts of the detector from one exposure to the other. The tar-

get source was always close to the center of the CCD (within about 100 pixels). Typical exposure times were between 120 and 600 sec, depending on seeing and target brightness. No photometric standards were observed, and observations sometimes were performed in non-photometric conditions.

In addition to the target fields a number of astrometric calibration fields were also observed in each run. Overlapping frames with large separations of about 1/3 of the field-of-view (FOV) were taken in a 2 by 2 or 3 by 3 pattern with typically 200 sec exposures. All these fields are at low galactic latitude to provide a high star density, but are not too crowded in order to avoid large numbers of blended images. These fields significantly enhance the number of residuals available later in the astrometric reductions to produce field distortion maps. They also often contain a detected ICRF counterpart and allow comparison of results between different observing runs.

2.2. USNO astrograph

The same telescope which produced the USNO CCD Astrograph Catalog (UCAC) was also used to image a square degree area around each ICRF target at about the same epoch as the deep CCD imaging runs. Some observing statistics for this investigation are given in Table 2. Properties of the astrograph and its camera are given in Table 3. The imaging optics is the 5-element “red lens” with a design FOV of 9° diameter, thus the entire 4k by 4k CCD area is practically “on the optical axis” with very uniform image quality.

Typically sets of 4 long (150 sec) and 4 short (30 sec) exposures were taken with the astrograph on one side of the pier, with an offset of about 1/4 of the FOV in a 2 by 2 pattern centered on the target. A similar set of exposures was taken with the telescope flipped to the other side of the pier. This approach compensates for possible constant, magnitude dependent systematic errors of derived star positions. For some fields fewer numbers of exposures were taken, however, always aiming at a balance between East and West of pier observations.

Important to note is that although the same instrument was used, none of the astrograph observations used for this ICRF investigation are part

of the published UCAC star catalogs. The special observing performed for this investigation has a much larger number of exposures per field than the general UCAC survey data, the additional benefit of symmetric East and West of pier observations, and a somewhat increased exposure time for better signal-to-noise performance of faint stars.

3. Data Processing

3.1. Astrograph data processing

The pixel-to-pixel sensitivity variations of the 4k CCD are small and could be well corrected with mean flats. No separate bias corrections were applied beyond what has been corrected by applying the dark frame calibrations. Image centers were obtained from fits of the calibrated pixel data with a 5-parameter, 2-dimensional image profile model. For the UCAC2 a Gauss function profile model was used followed by correction of x, y data for the pixel-phase error (Zacharias et al. 2004). For UCAC4 a better matching modified Lorentz profile was utilized for the image profile model function, using fixed shape parameters determined from pilot investigations but using only 5 free parameters for individual star fits in the final reduction (Zacharias 2010).

The astrograph data were initially processed following the procedures of the UCAC2 reduction pipeline (Zacharias et al. 2004), hereafter called UCAC2-type. Later the raw data were re-processed with methods adopted for UCAC4 (Zacharias et al. 2013), drawing upon the UCAC3 pipeline ((1)) for most of the code, hereafter called UCAC4-type. Note that in neither case actual UCAC2 or UCAC4 catalog data were used for these reference stars, rather dedicated, extra astrograph observations were processed with respective pipelines.

Due to the poor charge transfer efficiency (CTE) of the 4k CCD used at the astrograph, the camera was operated at a relatively warm temperature of about -18° C to mitigate the problem. The resulting high dark current required frequently constructing mean dark frames for the standard exposure times involved. Nevertheless a significant coma-like systematic error exists in the astrograph data for the x -coordinate. Elaborate corrections were applied to reduce the initial systematic errors on the 100 mas level to about 10

mas. Detailed procedures to correct for CTE effects were different between the UCAC2-type and UCAC4-type reductions (see above cited papers).

The models for these corrections were developed by utilizing 2MASS (Skrutskie et al. 2006) reference stars for differential astrometry, spanning the entire magnitude range available with the astrograph data. No proper motions of 2MASS stars were available. However, the mean epoch difference between the 2MASS catalog and the astrograph data is typically about a year thus global galactic kinematic effects are irrelevant here over scales of the size of an astrograph exposure. We were looking only for position differences as a function of magnitude and x, y coordinates on a 1° scale. The large number of residuals (typically thousands for a parameter space bin) allowed the large noise (order 80 mas, 1σ) of individual star position differences to be reduced to insignificant levels as compared to the systematic error calibration goal of about 10 mas. Utilizing East and West of pier observations for this investigation further reduces the remaining effects of the poor CTE in the astrograph data.

After applying these systematic error corrections to the x, y centers of fitted stars an astrometric solution was performed using the Tycho-2 (Høg et al. 2000) as reference star catalog. However, stars fainter than about magnitude 11 were excluded, as these were found to be of lower astrometric quality than the rest of the catalog. A linear plate model was used in these reductions after handling atmospheric refraction and aberration rigorously with our custom code. In an iterative process a field distortion map was constructed from the residuals and binned by x, y coordinates. A smoothed version of this map was applied to the data before the final astrometric solution with the same “plate” model. A secondary reference star catalog was then generated from the weighted mean positions of stars from all astrograph observations of these ICRF fields, covering the about 10 to 16 mag range in our bandpass.

3.2. Deep CCD data reduction

Raw data processing of the deep exposures was performed with IRAF. Mean bias and dome flat frames were applied for calibration. Each exposure was checked for image quality like astigmatism related to focus and mean image elongation related

to guiding effects. The target source was identified using finding charts and the source checked for blended images, cosmic ray hits or other problems. Notes were made and flags set to exclude individual exposures of questionable quality.

For the astrometric reductions of the deep CCD exposures the secondary reference star catalog from the astrograph observations was used. Again, atmospheric refraction and aberration as function of x, y and telescope pointing were handled rigorously. A weighted least-squares reduction was performed, considering the formal x, y fit errors of individual stars, an error contribution from the turbulence of the atmosphere (scaled by the inverse square-root of exposure time), and the formal errors of individual reference star position coordinates.

Various plate models were explored and a significant 3rd order optical distortion found, as expected for this type of optics. The x, y data, for each telescope and observing run separately, was then pre-corrected for the mean optical distortion term and astrometric reductions repeated with a linear model. Residuals were then binned as function of x, y coordinates in the focal plane and a smoothed map generated from all data of an individual observing run. An example of such a field distortion pattern is shown in Fig. 2 presenting data from the CTIO 0.9 m telescope observing run “q” based on UCAC4-type reference stars. Over 40,000 residuals from 279 exposures were used for this vector plot. These corrections were applied to the x, y data of individual exposures and the astrometric reductions repeated with the same model and distortion pre-corrections. Due to degraded optical quality far from the optical axis, reference stars in the corners of the CCD were excluded from the final astrometric reductions.

3.3. Total random error of optical positions of targets

The total optical position error of our ICRF counterpart targets per coordinate, and per individual deep CCD exposure, σ_{tot_i} , from all known, random error contributions is

$$\sigma_{tot_i} = \sqrt{\sigma_{xyfit}^2 + \sigma_{as}^2 + (100mas)^2 \frac{100sec}{t_{exp}[sec]}}$$

Included here are the x, y position fit error of the

target source on individual deep exposures, σ_{xyfit} , the contribution from the error propagation of the astrometric solution, σ_{as} , see below, and the error from the turbulence in the atmosphere for the target source. The last term scales with exposure time, t_{exp} , depends slightly on the angular distance of the target to the reference stars, and is correlated with the “astrometric seeing”. An estimate is adopted here based on previous observational data with the 0.9 m CTIO telescope (Zacharias 1996). This term represents the random offset of the observed center of the target source w.r.t. its true position on the grid of reference stars, caused by the turbulence in the atmosphere. The total, random error of a mean target position from optical data, σ_{tot} , as given in the results tables below then is the weighted mean of the above over all contributing exposures.

Turbulence in the atmosphere of course also contributes to the astrometric solution error by affecting the reference stars. This and the random catalog position errors of the reference stars and the random x, y fit errors of the reference stars are automatically included in the formula for the error contribution from the astrometric solution, σ_{as} (spelled out here for the ξ coordinate),

$$\sigma_{as}^2 = \sum_{i=1}^k \left(\frac{\partial \xi}{\partial p_i} \right)^2 \sigma_{p_i}^2$$

The formula for the η coordinate is similar, with ξ, η being the standard coordinates in the tangential plane. Here σ_{p_i} are the errors of the $i = 1, k$ “plate constants” of the adopted astrometric model between the standard coordinates, and the observed x, y image center coordinates of those reference stars. All error sources mentioned above contribute to the astrometric solution error. The partial derivatives by plate constants depend on the adopted model and are evaluated at the position of the target extragalactic source on a given deep CCD exposure. In other words, σ_{as} is the error contribution from the error propagation of the astrometric solution process in the tangential plane, i.e. the error associated with how well the coordinate system represented by the reference stars in the field of view is established at the point of the target source on a given deep exposure.

4. Results

Weighted mean optical positions (per observing run) of ICRF counterparts were derived by the procedures described above, excluding deep exposures of questionable quality. For most sources UCAC2-type and UCAC4-type reductions were performed (see section 3.1). The optical reference frame used is the Tycho-2 catalog, excluding its faintest stars. Thus the optical positions presented here should be on the HCRS. These positions are compared to the radio positions using the ICRF2 (Fey et al. 2009) data. The optical–radio position differences and associated errors are analyzed further as described below.

4.1. Optical position tables

The primary results of this investigation are presented in Tables 4 and 5, for the UCAC2 and UCAC4-type reductions, respectively. The full tables are available from the CDS in Strasbourg (Zacharias & Zacharias 2013), while a sample is given here. Both tables are in the same format. The tables contain 666 and 682 lines (position results), respectively for a total of 413 unique sources. Many sources were observed in more than one observing run. Not all sources were reduced with both types of secondary reference stars.

Columns 1 and 2 list the optical positions, RA and Dec [hms format], respectively for individual sources and observing runs as derived from this investigation. Those positions are on the Tycho-2 coordinate system believed to be on the Hipparcos Celestial Reference Frame, which in turn is constructed to be on the ICRF. Columns 3 and 4 give the same position in decimal degree format. Column 5 is the radial distance [mas] between the optical and radio position based on columns 6 and 7, which give the position differences optical minus radio, $\Delta\alpha \cos\delta$, $\Delta\delta$, respectively [mas]. Data from the published ICRF2 catalog (Fey et al. 2009) were used for the radio positions.

Columns 8 and 9 give the total optical position error per coordinate, as discussed in section 3.3. Particularly the x , y -fit errors can vary significantly due to differences in signal-to-noise (S/N) ratios of observed sources as well as the number and quality of available reference stars. However, due to the circular symmetric nature of the image

profile fit function the x coordinate and y coordinate errors are equal. Similarly, error propagation values from σ_{as} are almost the same for both coordinates, leading to identical values in columns 8 and 9 when rounded to mas.

Column 10 gives the ratio of columns 6 and 8, i.e. the optical–radio position difference for RA in unit of “sigmas”. Column 11 gives the same for the Dec component. Column 12 gives the error of the radio position [mas] (per coordinate; the larger of the RA or Dec component is shown) from the ICRF2. In almost all cases this error is negligible as compared to the optical position errors. A value of 99 indicates an unknown error.

Column 13 gives the number of deep exposures used for the mean, optical position of this source and run. Column 14 provides the average number of secondary reference stars used for this field in the deep CCD reductions, and column 15 lists the number of reference stars excluded (above the adopted 3σ threshold of astrometric solution error). Column 16 gives the mean astrometric plate solution error [mas] from the individual deep exposures. Column 17 gives the approximate S/N ratio of the optical counterpart image on a single deep exposure.

Column 18 and 19 give the optical brightness and redshift, respectively, taken from the LQAC-2 (Souhay et al. 2012) catalog. If available the R magnitude is used, otherwise, in order of preference, I, V, or g. Zero in this column indicates that no magnitude was available from the above options. Column 20 gives the object type 1, 2 or 3 for AGN, BL-Lac, or QSO, respectively, according to the 13th edition of (Veron-Cetty & Veron 2010).

Column 21 lists the X-band radio structure index. A value of 1 indicates an (almost) point-like source, while 5 means a lot of structure is seen. A value of 9 indicates an unknown radio structure index. A combination of 3 data sets are used, with the Bordeaux database (Charlot 2013) as first pick, followed by a recently published table (Bourda et al. 2011) and the ICRF-2 catalog data.

Column 22 is either 2 or 4 to indicate the UCAC2 or UCAC4-type solution. This allows the user to merge and sort both tables if desired, while retaining that information for each row. Column 23 gives the B1950 coordinate-based name of

the source taken from the ICRF2, which is commonly used in the VLBI community. To obtain the J2000-based, IAU-style name of a source, just use columns 1 and 2 to the desired level of digits.

Column 24 contains the 1-letter name of the deep CCD observing run (see Table 1), while column 25 is either “r” for a regular radio-optical reference frame source in our program, or “c” indicating also an optical calibration field (see above). The flag in column 26 indicates the quality of the optical source image, with possible values explained in Table 6. The label “n” is used for 2 sources not being in the ICRF. Radio positions were taken as follows for 0447–439 (Perlman et al. 1998) and 2316–423 (Roopesh, priv.com.). Finally, column 27 contains remarks, e.g. if the optical image looks like a resolved galaxy or is a double, in which case the flux ratio ($f_{lr} = \text{target source} / \text{component}$) and separation (arc-sec) are given.

4.2. Empty fields

Table 7 lists the ICRF sources where an optical counterpart within an arcsec of the radio position could not be found to a limiting magnitude of about $R = 22$ (in most cases, sometime 20 to 21 with Moon and/or poor seeing). In some of those cases, particularly in crowded fields at low galactic latitudes, a nearby point source was found, but accurate astrometry rules out the possibility of a positive match with the ICRF source. In most cases the position offset from the optical object (likely foreground star) to the ICRF radio position is given in the comment column of Table 7. Some of these fields had more than 1 observing run attempt to find an optical counterpart. The area around ICRF source 0826–373 was targeted as one of the field distortion calibration fields imaged during several observing runs.

4.3. Global system orientation

It is possible that the optical coordinate system as represented by Tycho-2 stars in our investigation at around epoch 2000 is no longer perfectly aligned with the ICRF radio coordinate system. Allowing for 3 Eulerian, rigid body, rotation angles (as transformation between the 2 static coordinate systems) in a least-squares solution of our optical minus radio position differences we find marginal

significant results. No attempt has been made to also solve for a system rotation (change of orientation with time) due to the short time baseline of our observing epochs.

For comparison some solutions were obtained with an additional fit parameter, a constant offset in declination. Most of our sources are in the southern hemisphere and such an offset is conceivable, perhaps introduced by remaining systematic errors as a function of magnitude. The difference in brightness between our primary reference stars (Tycho-2) and the ICRF optical counterparts is almost 10 magnitudes and a very small remaining magnitude equation could produce such a global offset in declination. If present, a similar offset in RA is already covered by the 3rd orientation angle around the z coordinate axis.

Table 8 summarizes the results of various solutions, giving the Eulerian angles w_1 to w_3 , declination offset (if solved for), and the errors of those parameters. The first column gives the fit error followed by the number of degrees of freedom (number of observation equations used minus number of parameters to solve for). The last column distinguishes between different solutions, with u and w indicating unweighted and weighted solutions, respectively. The number 2 or 4 indicates UCAC2-type or UCAC4-type data. The “3sig” indicates that observation equations with residuals above 3σ are excluded and limits of 150 mas and 30 mas are put on optical–radio offsets and radio position errors, respectively. Similarly the less restrictive “4sig” excludes observation equations only if above 4σ and adopts 200 mas and 90 mas for the selection criteria mentioned above.

Depending on selection criteria for these solutions one can get quite different results. However, there seems to be a consistent trend with about +5, –4, and +5 mas for the angles 1 to 3, and –4 mas for the declination offset, with formal errors of about 1.5 mas each. These values are slightly larger than expected from the alignment tolerances of the HCRS to ICRF systems alone (Kovalevsky et al. 1997) which give a spin error of 0.25 mas/yr (1σ) leading to an expected offset of just over 2 mas over the approximately 9 year mean epoch difference between Hipparcos (1991) and our data (2000).

For the following statistics we do not correct

our optical–radio position differences for this possible global orientation misalignment, but rather use the data as given in our optical–radio catalog (samples shown in Table 4 and 5).

5. Analysis of optical minus radio position differences

5.1. Precision of position differences

Fig. 3 shows the distribution of our formal, optical position errors of the RA coordinate for the UCAC2-type reductions. These errors include the x, y position fit error of the sources, atmospheric turbulence and error propagation from reference star errors and “plate” solutions of both steps in the reductions. These errors are for the mean optical position of a target source over all exposures of a given observing run. Results for Dec and for the UCAC4-type reductions are almost identical. The high precision of our observations is apparent with most sources falling in the 10 to 15 mas bin.

In the following we exclude source observations by 3 criteria: optical minus radio position differences exceeding 100 mas (in either coordinate), $f\sigma$ (columns 7,8 of tables 4 and 5) exceeding 3.5, and low S/N sources (≤ 5). With this we get a root-mean-square (RMS) optical–radio position offset of 24.2 and 24.3 mas for the RA and Dec component, respectively for the UCAC2-type solution. In these statistics 501 out of 666 source observations of table 4 are included (306 individual sources). The corresponding numbers for the UCAC4-type solution are 27.1 and 26.0 mas for 506 out of 682 source observations and 317 individual sources. This result makes our investigation the most precise of its kind published so far.

Fig. 4 shows a histogram of the UCAC2-type optical–radio position differences of all of our data, while Fig. 5 shows the same for the UCAC4-type data. Individual sources in this set have significantly different S/N and thus significantly different image fit precisions and total errors. Thus individual observations come from different statistical populations and Figs. 4 and 5 can’t be expected to be normal distributed.

5.2. Underestimation of formal errors

Figs. 6 and 7 show histograms of the same data as Figs. 4 and 5 but scaled for individual errors,

i.e. the distribution of (optical–radio) position differences divided by the total, known (1σ) error for that observation. If the error estimates were correct and the position differences were normal-distributed, then the histogram data would be consistent with a Gaussian function of standard deviation 1.0. The curve plotted over the histograms in Figs. 6 and 7 are the best fit Gauss functions, however the standard deviations are 1.25 and 1.29 for the RA and Dec component of the UCAC2-type data respectively, and 1.40 and 1.33 for the UCAC4-type data. Here outliers were excluded, using 545 data points out of 666 and 541 out of 682 for the UCAC2 and UCAC4-type data, respectively. Including these outliers the best fit distributions would be even wider.

Thus these distributions are about 30% wider than expected from known error sources. Furthermore all distributions are “heavy tailed” even when compared to the already broader best fit normal distribution. A large number of sources are above 3σ , consistent with what is seen in other investigations of this type. As already indicated from the global system rotation analysis (see above) Figs. 6 and 7 also show that the means of these distributions are slightly offset from zero.

Table 9 lists the 88 observations of 63 sources with (optical–radio) position differences over 4.0σ (of total, formal error as listed in Table 4) in either coordinate from our UCAC2-type data. This corresponds roughly to 3σ outliers assuming the best fit Gaussian distribution as shown in Fig. 6 and 7. The format is the same as that of Table 4. These include several “problem” sources, as can be seen from the comment column. A few might even be “no match” cases. Some other entries in Table 9 are sources with moderate (optical–radio) position offsets (50 to 100 mas) where very small, total, formal optical position errors result in exceeding the 4σ threshold. The corresponding list from the UCAC4-type data (not shown here) is very similar and can be obtained by selecting from the published full data catalog (Zacharias & Zacharias 2013) (sample shown in Table 5).

There are 2 possible causes which could explain the larger than expected optical–radio position differences: systematic errors in the optical reference star data, and astrophysical non-coincidence of the optical and radio centers of emission. As

shown below there are strong indications for the presence of both explanations. Systematic errors in the radio reference frame are much smaller than the 20 to 200 mas level needed to explain the position discrepancies.

5.3. Vector plots

The key results of our main tables 4 and 5 are visualized in Fig. 8 and 9 showing the location of our sources on the sky together with vectors indicating the optical–radio position differences. Fig. 8 shows the RA range of 0 to 12 hours, while Fig. 9 shows the 12 to 24 hours area (each with some overlap). The scale of the vectors is 10 mas per degree. The red and blue vectors show the results of the UCAC2 and UCAC4-type reductions, respectively. Excluded from these plots are sources with formal errors or position differences exceeding 200 mas per coordinate. The few sources with excessive position differences are discussed below. In many local areas the vectors seem to be aligned, indicating systematic errors related to the reference stars.

5.4. Systematic errors in the optical data

The primary optical reference frame used in this investigation is the Tycho-2 (Høg et al. 2000) star catalog. The mean positions of stars in the Tycho-2 catalog are based on Hipparcos space mission observations at central epoch 1991.25. However, the Tycho-2 proper motions were derived in combination with many early epoch ground-based catalogs, of which the Astrographic Catalogue (AC) project from the 1900s is of particular importance because of the large epoch difference, its high precision and coverage of the 9 to 11 mag range, i.e. the stars used as primary reference stars in our investigation.

The AC data consists of some 20,000 photographic plates of about 2.1 by 2.1 degree size, taken in a 2-fold overlap pattern (center in corner), with plate centers on each full degree of declination (Eichhorn 1974). These AC measures were reduced with great care using Hipparcos reference stars (Urban et al. 1998). However, removing systematic errors, particularly those depending on magnitude and products of magnitude and x, y coordinate (coma terms) was limited to about 100 to 200 mas (Urban, private comm.) The correspond-

ing error floor of the Tycho-2 proper motions thus is in the order of 1 to 2 mas/yr, possibly varying over scales of 1 degree (distance from center to edge on an AC plate). This translates to remaining, typical, systematic errors from the Tycho-2 catalog of 10 to 20 mas for reference stars at our mean 2000 epoch of optical counterpart observations (9 years after the Tycho-2 central epoch). In addition, the USNO CCD Astrograph observations are affected by remaining systematic errors on the same 10 to 20 mas level due to the poor charge transfer efficiency of the CCD detector used (Zacharias 2010). The size of the astrograph field-of-view is 1 by 1 degree. From both sources, the Tycho-2 and the astrograph observations, we have possible systematic positional errors on the 10 to 20 mas level, while there is no indication of remaining systematic errors in our deep CCD imaging data on the 10 mas or larger level.

In order to probe for small-scale correlations of optical–radio position differences we produced a list of all nearest neighbor cases, up to about a 1.2 degree separation, which are shown in Table 10. All sources which have optical–radio position differences exceeding about 1.5 times their total, formal error in either coordinate are marked in the last column referring to the figure number of a zoomed-in sky plot showing the location of those sources, the optical–radio position difference vectors, and the total, formal error (circles). In Figs. 10, 11, and 12, data from the UCAC2-type reductions are shown in red, while those of the UCAC4-type are in blue. Note, for many sources the errors for both types of reductions for a given source and observing run are the same (rounded to nearest mas), and the blue color overwrites a red circle in those cases.

Fig. 10 shows an area containing 3 sources (0403–132, 0405–123, and 0406–127 from left to right) all within about 1 degree on the sky. For all sources more than one observation was performed at different epochs and results from all such observing runs are shown by multiple vectors and error circles. Individual vectors per source show consistent results independent of the UCAC2 or UCAC4 type reduction and observing run. There is no reason to believe that all optical centers of emissions are offset from the radio centers by about the same amount and direction for those 3 different QSOs. However, the observed

optical–radio position offsets of 0405–123, and 0406–127 are the same (within the errors) and those of 0403–132 are of similar amplitude but with inverted direction. Note that different Astrographic Catalogue plates (shown as large squares in Fig. 10) cover this area of sky, with source 0403–132 being on the northern edge of the southern plate (with a plate center near -14°) while the 2 other sources are just south of the more northern plate center. Remaining systematic errors from a coma term in the reductions of those plates could explain the change of sign around declination -13° .

Figs. 11 and 12 show the other 2 cases of neighboring sources in our sample with significant optical–radio position differences. The most northerly source in Fig. 12 does not provide any insight because the errors are much larger than the optical–radio position difference. The other 2 sources in Fig. 12 show some large optical–radio position differences along similar directions, while the data from Fig. 11 do not. The amplitude of optical–radio position offsets seen in our data is well within the expected, remaining, local systematic errors of Tycho-2 reference stars at our observing epoch (see above).

Looking at all results (Figs. 8 to 12) indicates that remaining systematic errors in the reference stars (Tycho-2 proper motions via Astrographic Catalogue, and possibly also UCAC data) could very well explain at least some of the larger than expected (from all known formal errors) optical–radio position differences. Using spherical harmonics analysis on the entire southern hemisphere is unlikely to give more insight into this problem. Large-scale zonal patterns might be revealed; however, apparently small-scale variations of systematic errors over just 1 to 2 degrees seem to play a major role and the number of sources is insufficient to characterize errors on such small scales with spherical harmonics.

5.5. Physical offset of optical and radio centers of emissions

Are there other explanations which might explain part of the larger than expected optical–radio position differences than issues with optical positions of reference stars? The answer is yes, there are indications for actual physical position offsets between radio centers and optical counterpart cen-

ters.

The first indication comes from sources with very large optical–radio position differences (4). Source 0648–165 was observed twice with formal errors of 30 and 70 mas per coordinate, respectively, while the optical–radio offsets are consistently about 300 to 400 mas per coordinate. This is much larger than could be explained from remaining systematic errors in some reference stars.

Another example is 1345+125, a Seyfert galaxy with visible host galaxy and 2 nuclei, separated by about 2 arcsec (O’Dea et al. 2000), resulting in our observed optical–radio position offset of about 1.3 arcsec from data taken in about 1.5 arcsec seeing which did not resolve the components. A similar blended image example is 1730–130 which was not resolved in one of our observing runs and resulted in over 400 mas optical–radio position offset, while special point spread function (PSF) handling of data from another observing run with better seeing allowed the blended image to be resolved, resulting in an optical position coinciding with the radio source position within the formal errors of about 30 mas.

Other investigations also find such outlier cases (see below), which could be explained by some abnormality in the optical structure (blended images, optical galaxy core not coincident with radio peak etc.). The question is, do we only have to exclude such sources and arrive at a “clean” set of sources with no physical position offsets between centers of radio and optical images, after which all the remaining excess in optical–radio position offsets can be explained by reference star issues? The answer is likely no, as we will see next.

The ratios of our optical–radio position differences and their formal errors (per coordinate) were used for the following, excluding 6σ and larger outliers. Fig. 13 shows the RMS scatter of those ratios (binned by 16 sources) as a function of redshift, while Fig. 14 shows the same as a function of X-band radio structure index. There is an obvious trend toward smaller optical–radio position differences for larger redshifts and smaller radio structure index. This somewhat surprising result confirms earlier findings of this nature (da Silva Neto 2002). This effect can not be explained by systematic errors in reference star catalogs, and contradicts the assumption that optical and radio centers of emissions are coincid-

ing on the mas level independent of radio structure or distance (redshift) of the sources. However, the radio structure is only on the (sub)mas level while the observed unexplained excess in the optical–radio position offsets are 1 to 2 orders of magnitude larger. Similar to the connection between the mass of the black hole in the center of galaxies and the overall size of the galaxy, there seems to be some connection between small-scale radio structure and larger scale optical–radio position offsets.

6. Comparison to other projects

A comparison to (Camargo et al. 2012) is not made here due to the small number of sources (22) in common and relatively high optical position errors (80 mas). A recent paper (Orosz & Frey 2013) published optical positions of over 1200 ICRF2 counterparts based on SDSS observations. However, no source in common was found between these (mostly northern hemisphere) and our observations (mostly southern hemisphere and original ICRF sources).

A total of 281 sources of the 300 sources in the Rio survey (Assafin et al. 2013) are in common with our observations. The unweighted, mean position differences of our optical observations to those of the Rio survey are -3.3 and -8.1 mas for the RA and Dec component, respectively when using the UCAC2-type reductions. The RMS scatter for these differences (excluding individual position differences larger than 200 mas) are 43 mas per coordinate. Using the UCAC4-type reductions the mean position differences with the Rio survey are -1.5 and -6.5 mas for RA and Dec, respectively with an RMS scatter of 45 mas per coordinate.

Fig. 15 shows the optical–radio position differences as observed by the Rio survey versus that of our observations. As expected there is some correlation, both sets of data point to similar optical–radio position differences because both are based ultimately on the Tycho-2 optical reference frame with some sort of UCAC data for intermediate reference stars, and the deep CCD imaging has the same resolution and similar mean epoch of observation in both cases. However, this comparison does not help us to distinguish between reference stars systematic errors and possible physical position offsets between the radio

and optical centers of emissions.

As part of the Hipparcos to ICRF coordinate system link the separation between pairs of selected QSOs and nearby Hipparcos stars was measured with the HST Fine Guidance Sensors (FGS) (Hemenway et al. 1997). System orientation and rotation (spin) angles (6 parameters) were determined with an accuracy of about 2 mas (2.5 mas/yr) from observations of about 40 pairs. Elaborate calibrations to the FGS data were applied related to interferometer null, coordinate system drift, and changes in field angle distortions. Nevertheless the input variances of both the formal errors of Hipparcos proper motions as well as the formal errors of the FGS observations had to be scaled by a factor of 4 to match the error budget of the solution. Post-fit residuals on the 10 mas level were observed, significantly larger than the expected formal errors. An individual target, for some yet unknown reason, had to be excluded which changed the entire solution by over 10 mas/yr for the rotation around the z -axis.

Another interesting clue comes from comparing the number of “outliers” to the sample size of various investigations when considering the optical observation precision. The comparison of SDSS optical positions with ICRF2 radio sources (Orosz & Frey 2013) finds 51 “outlier” sources (over 3σ of formal errors) out of 1297 sources total, i.e. about 4% of the optical position data at about the 60 mas precision level. Both this paper and our investigation explicitly list all the outliers found, while the Rio survey (Assafin et al. 2013) of 300 sources was cleaned up before publication and does not list any sources with optical–radio position offsets over 3σ . The precision of the Rio survey is about 52 mas per coordinate when RMS combining the source centroid errors and zero-point errors from the “plate” reduction process.

For our UCAC2-based data we find 145 observations out of a total of 666 where at least 1 coordinate has an optical–radio position offset of 3σ or more of the total, estimated random position error. These belong to 104 unique sources out of 371 sources, thus about 28% are “outliers” under this definition. For the UCAC4-based results we see similar numbers: 156 observations over 3σ out of 682 total, for 113 unique sources out of 392, or 29%. If we attribute some of the unexplained er-

rors to reference star issues and assume the above mentioned best fit Gaussian curve to the observed optical–radio positions (thus increasing our error budget by about a factor of 4/3) that leaves us with about 63 “outlier” sources (Table 9) out of a total of 371, which is 17%.

6.1. Are all sources “problem cases” ?

Thus between our data and the SDSS/ICRF2 investigation we see an increase in the percentage of “outliers” by about a factor of $20/4 = 5$ for an increase in survey precision by about a factor of 2 (60 mas of SDSS/ICRF2 data versus 30 mas of our observations). If this trend continues (ratio of percent increasing proportional to ratio of survey precision) we would reach a 100% “outlier” level for another precision factor of 2, thus for a survey of about 15 mas precision per coordinate. Note that many of our “outlier” sources are among the higher than average precision observations, i.e. drawn from about 10 mas 1σ position error samples. A 3σ on that would be about 30 mas. A survey similar to ours but 2 times more precise would thus show most sources to be “outliers” on the 15 mas level.

This leads us to the DARN hypothesis (detrimental astrophysical random noise) of optical–radio position differences: For most ICRF-type sources the optical and radio centers of emission are randomly offset by order of ≈ 10 mas due to inherent astrophysical source structure effects (when imaged in the optical with a resolution too low to actually see individual structure, and thus the direction and amplitude of possible offsets).

Is this possible? At typical distances of these ICRF quasars ($z = 0.5$ to 4) the standard cosmological model predicts an angular distance of about 1 Gpc within a factor of 2 (Beckmann & Shrader), thus a separation of features of 1 kpc corresponds to about 200 mas. The brightness of host galaxies at optical wavelengths is typically 10% of that of the dominant core of such AGNs, see for example an imaging study with HST of $z = 2$ QSOs (Hutchings et al. 2002). There is no reason to believe that the optical light distribution of such a host galaxy is perfectly (on percent-level) symmetric and centered on the radio core position. A near-IR adaptive optics study finds about 30% of QSO host galaxies disturbed (2), which is not surprising considering the cause of

AGNs related to merging galaxies. The typical radius of AGN host galaxies is about 10 kpc (Beckmann & Shrader). Variations of optical light distributions (spiral arms, dust, asymmetry or small offsets of halos in elliptical galaxies) could be on the kpc scale. Assuming the combined center of optical light of this about 10 kpc radius structure is offset by a mere 0.5 kpc from the radio emission center (QSO black hole core), this translates to an angular offset of 100 mas (see above). With about 10% of the light contribution by the host galaxy the optical centroid of the combined light from host galaxy and QSO would be shifted by about 10 mas from the radio position when the optical structure can not be resolved (would need about 10 mas resolution and high dynamic range). This seems like a possible if not even plausible scenario, at least for “disturbed” galaxies, while the effect will be less for more symmetric, elliptical galaxies.

We do not know the distribution of the true optical–radio centers of emission offsets. A significant fraction of sources could have offsets much smaller than 10 mas - we just don’t know at this time. Gaia will be able to answer this. It is doubtful that the problem of non-coincidence of optical and radio centers of emissions can be mitigated by using better fitting algorithms, see e.g. a discussion in (Makarov et al. 2012), if the disturbance causing the optical position offset is within the angular resolution limit of the optical data.

A general increase in optical–radio position offsets noise on the 10 mas level could of course come from remaining systematic errors in reference star positions. The amount of this error amplitude is well within the expected, remaining systematic errors from reference stars, and if indeed degree-scale variations of these errors on the sky exist, as indicated from the above discussion, they would appear as random noise in our data. However, that would not explain the correlations of the observed optical–radio position offsets as a function of radio structure index or redshift, nor the larger than expected errors in the HST investigation for the Hipparcos frame alignment. Also, clear cases with astrophysically caused offsets of optical and radio centers of emissions are seen on the 100 to 1000 mas level for a few (often nearby) sources. There is no reason to believe that the relative number of those sources will decline when looking at

smaller observed offsets - rather the contrary is to be expected. The few sources with over 100 mas astrophysically caused optical–radio position offset might very well be the tip of the iceberg.

For any radio to optical reference frame link effort, the errors to be considered for a single object would be the RMS sum of 3 components: the observed position errors in the radio, the corresponding errors in the optical data and DARN. Most ICRF radio position errors are on the order of 1 mas or less, and the optical position errors expected from the upcoming Gaia mission are on a similar level, which means the optical–radio reference frame link of these 2 systems would be dominated by DARN. Optical position shifts caused by variability of quasars linked to their inner structure (Popovic et al. 2012) are likely on smaller angular scales than DARN and thus might be overshadowed by DARN.

6.2. Next steps

In order to be better able to separate effects introduced by systematic errors of reference stars and possible, astrophysical non-coincidence of the radio and optical centers of emission, another observing run at the 0.9 m CTIO telescope was performed in March 2013. Systematic errors in the reference stars are mostly expected to come from proper motion errors. For the data presented in this investigation we had to bridge about 2000 – 1991 = 9 years of Tycho-2 proper motions, while the new observations have to bridge 2013 – 1991 = 22 years. This should lead to a significant increase in the optical–radio position differences if indeed reference star issues are dominant. Any optical structure induced optical–radio position offsets of our sources are expected to stay the same because patterns in the host galaxy can only change over much longer timescales. Of course the random errors from proper motion errors also increase and secondary reference stars were observed with a different telescope (URAT, <http://www.usno.navy.mil/USNO/astrometry/optical-IR-prod/urat>) this time, making the interpretation of the data more complex. Possible short-term photometric variability of AGN cores can shift the observed optical center of light as well, e.g. (Taris et al. 2010), complicating the situation further. Results from the new observations will be published in an upcoming paper.

Conclusive results in this matter will come from Gaia observations. The internal errors of optical positions are sub-mas even for the faint QSO targets. However, if DARN is confirmed, the hoped for accuracy of the alignment of the Gaia to the ICRF frame can not be achieved by an order of magnitude or more. Selecting a “clean” sample e.g. by monitoring optical variability (Taris et al. 2013) will not help when a significant and unknown optical–radio position offset exists on top of possible image shift variations. Small time-scale variations will be related to the AGN core, while a general position offset is caused by the asymmetry of the host galaxy’s light distribution.

A better link of the Gaia and ICRF reference frame will come from observing more sources. Finding more optically bright QSOs among radio sources (Petrov 2013) is an option. Deep ground-based imaging can determine positions of optically faint ICRF2 sources using Gaia reference stars, even if the targets are too faint to be observed with Gaia. Finding more extragalactic radio sources with optical counterparts will help, even if position errors are relatively large (10 mas level).

7. Conclusions

Based on the results and discussions presented in this paper we can draw the following conclusions:

1. This investigation is the most precise of its kind so far with a formal mean error of 25 mas per coordinate for the optical positions of ICRF counterparts. This was achieved from well calibrated astrometric observations with mostly the 0.9 m CTIO telescope in combination with contemporary astrograph observations providing intermediate bright reference stars on the Tycho-2 (Hipparcos) coordinate system (HCRS) at the same epoch as the deep imaging data.
2. This sets an upper limit of about 25 mas (1σ) of possible non-coincidence of the optical and radio centers of emissions of typical ICRF quasars, with a few outliers already seen well exceeding this level of positional precision.

3. Comparing UCAC2-type and UCAC4-type solutions, use of UCAC2-type reference stars result in slightly smaller scatter of the optical–radio position differences, while use of UCAC4-type reference stars show smaller offsets to the radio reference frame coordinate axes.
4. Larger than expected (from the combined, total, formal errors) optical–radio position offsets are seen, which in part can be explained by systematic errors in the reference stars, particularly errors in the Tycho-2 catalog changing on degree scales, likely due to limitations in calibrating magnitude equations and coma terms in the Astrographic Catalogue data.
5. Correlations of optical–radio position differences with redshift and radio structure index of sources, comparison of the number of “outliers” from optical surveys of different precisions, and examining Hipparcos to ICRF link observations by HST FGS involving QSO–star pairs indicate other contributions besides systematic errors in reference star positions. These indications lead to the hypothesis of a true, detrimental, astrophysical random noise (DARN) offset of radio and optical centers of emission on about the 10 mas level. Higher optical accuracy data is needed to conclusively prove this DARN hypothesis; however, besides the observational indications there is a possible astrophysical explanation for such an error contribution on that level due to host galaxy structure at optical wavelengths.
6. It is estimated that Gaia observations will provide a rigid, instrumental, optical reference frame on the few micro-arcsecond level (Lindgren et al. 2012). Its construction will not be affected by possible significant optical–radio position offsets of individual ICRF sources. However, the errors in alignment of the Gaia internal coordinate system to the ICRF will be affected by DARN, if it exists. Although the radio positions as well as the Gaia observed optical positions of ICRF sources in common will have sub-mas precision, DARN will dominate the error budget. If the mean optical–radio position offsets are indeed typically 10 mas and there are about 600 link sources (2 coordinates each) the 3 orientation angles of the Gaia frame each can only be determined to about 0.5 mas (1σ) precision with respect to the ICRF. Absolute proper motions and parallaxes will not be compromised, only absolute positions, if a rigid, instrumental Gaia system can be constructed without zonal errors.
7. If DARN exists and a higher positional alignment of the Gaia and ICRF reference frames is desired, more objects in common with sufficient radio and optical flux will be needed, instead of concentrating on a “clean” sample (i.e. small radio structure index, low optical variability), because the error contribution of an individual source for the radio to optical coordinate system link will be dominated by that unknown, random optical position offset. Ground-based observations of ICRF sources too faint to be seen with Gaia directly could provide optical positions on the Gaia system using Gaia reference stars to its limiting magnitude in small fields of view, using large aperture, long-focus telescopes. Determining radio positions of more targets observed by Gaia is another option. Radio or optical positions of those additional source observations would need to be only on or slightly better than the position error level of DARN (maybe 5 to 10 mas), to provide meaningful, additional data to improve the link of Gaia and ICRF reference frames. Monitoring programs to arrive at a “clean” sample would be of lower priority than the sheer number of “reasonably good” sources with both optical and radio positional data. The stability of an optical or radio position (below the DARN level) would not matter because of the unknown significant position offset between the centers of emission of optical and radio source.

CTIO and KPNO are thanked for having granted observing time and provided support for this project. We would like to thank everyone involved in this over a decade long project, particu-

larly all observers beyond the authors (T. Rafferty, E. Holdenried, and J. Perez). Charlie Finch is thanked for running the dedicated astrograph observations through the UCAC4 pipeline for many of the fields.

Ralph Gaume is thanked for supporting this project as Head of the Astrometry Department over the many years and under difficult budget constraints. National Optical Astronomy Observatories (NOAO) are acknowledged for IRAF, Smithsonian Astrophysical Observatory for DS9 image display software, and Tim Pearson at the California Institute of Technology for the *pgplot* software. More information about the UCAC and follow-up projects is available at www.usno.navy.mil/usno/astrometry/optical-IR-prod.

REFERENCES

- Assafin, M., Zacharias, N., Rafferty, T.J., Zacharias, M.I., da Silva Neto, D.N., Andrei, A.H., & Vieira Martins, R. 2003, AJ 125, 2728
- Assafin, M., Vieira-Martins, R., Andrei, A.H., Camargo, J.I.B., & da Silva Neto, D.N. 2013, MN 430, 2797
- Beckmann, V. & Shrader, C. 2012, “Active Galactic Nuclei”, Wiley-VCH, Weinheim, p. 265
- Browne, I. 2013, Mem. S.A.It. Vol. 75, 282
- Bourda, G., Colliouad, A., Charlot, P., Porcas, R.W., & Garrington, S.T. 2011, A&A, 526, 102
- Camargo, J.I.B., Andrei, A.H., Assafin, M., Vieira-Martins, R., & da Silva Neto, D.N. 2011, A&A 532, 115
- da Silva Neto, D.N., Andrei, A.H., Vieira Martins, R. & Assafin, M. 2002, AJ 124, 612
- Charlot, P. 2013, priv.com. Bordeaux radio structure index data, see also <http://www.obs.u-bordeaux1.fr/BVID/>
- Eichhorn, H. 1974, “Astronomy of star positions”, Fred.Ungar Publ., Michigan
- The Hipparcos and Tycho Catalogues, European Space Agency, publication SP-1200
- Fey, A., Gordon, D., & Jacobs, C.S. (Eds.), IERS Tech.Note 35, Frankfurt, 2009
- Finch, C., Zacharias, N., Wycoff, G. 2010, AJ, 139, 2200-2207
- Guyon, O., Sanders, D.B., & Stockton, A.N. 2006, New Astron. Rev. 50, p.748
- Hemenway, P.D. et al. 1997, AJ 114, 2796
- Høg, E., Fabricius, C., Makarov, V.V., Bastian, U., Schwekendiek, P., Wicencec, A., Urban, S., Corbin, T. & Wycoff, G.L. 2000, A&A 357, 367
- Hutchings, J.B., Frenette, D., Hanisch, R., Mo, J., Dumont, P.J., Redding, D.C. & Neff, S.G. 2002, AJ 123, 2936
- Kovalevsky, J., Lindegren, L., Perryman, M.A.C., et al. 1997, A&A 323, 620
- Lindegren, L., Lammers, U., Hobbs, D., O’Mullane, W., Bastian, U. & Hernandez, J. 2012, A&A 538, 78
- Makarov, V., Berghea, C, Boboltz, D., Dieck, C., Dorland, B., Dudik, R., Fey, A., Gaume, R., Lei, X., Schmidt, H., & Zacharias, N. 2012, Mem.S.A.It 83, 952
- O’Dea, C.P., et al. 2000, AJ 119, 478
- Orosz, G. & Frey, S. 2013, A&A 553, 13, arXiv:1303.6763
- Perlman, E.S., Padovani, P., Giommi, P., Sambruna, R., Jones, L.R., Tzioumis, A., & Reynolds, J. 1998, AJ 115, 1253
- Petrov, L. 2013, AJ 146, 5
- Popovic, I.C., Jovanovic, P., Stalevski, M., Anton, S., Andrei, A.H., Kovacevic, J., Baes, M. 2012, A&A 538, 107
- Skrutskie, M.F, Cutri, R.M., Stiening, R., et al. 2006, AJ, 131, 1163
- Souchay, J., Andrei, A.H., Barache, C., Bouquillon, S., Suchet, D. Taris, F., & Peralta, R. 2012, A&A 537, 99
- Taris, F., Souchay, J., Andrei, A.H., Bernard, M., Salabert, M., Bouquillon, S., Anton, S., Lambert, S.B., Gontier, A.M., & Barache, C. 2011, A&A 526, 25

- Taris, F., Andrei, A., Klotz, A., Vachier, F., Cote, R., Bouquillon, S., Souchay, J., Lambert, S., Anton, S., Bourda, G., & Coward, D. 2013, *A&A* 552, a98
- Urban, S.E., Corbin, T.E., Wycoff, G.L., Martin, J.C., Jackson, E.S., Zacharias, M.I., Hall, D.M. 1998, *AJ* 115, 1212
- Veron-Cetty, M.P., & Veron, P. 2010, *A&A* 518, 10
- Zacharias, M.I., Zacharias, N., & Rafferty, T.J., 2004, in *Proc. IAU XXV JD16*, Eds. R. Gaume, D. McCarthy, & J. Souchay
- Zacharias, M.I., & Zacharias, N. 2005, *ASP Conf.Ser.* 338, Eds. Kenneth Seidelman & Alice Monet, p. 184
- Zacharias, N. & Zacharias, M.I. 2008, in *proc. IAU Symp.* 248, Eds. Wenjing Jin, Imants Platais, & Michael A.C. Perryman, Cambridge University Press, p.332-333
- Zacharias, M.I. & Zacharias, N. 2009, poster paper at IAU GA Rio de Janeiro, www.ast.cam.ac.uk/iau_comm8/iau27/presentations/MZacharias.pdf
- Zacharias, M.I., Zacharias, N., & Finch, C. 2012, IAU GA Beijing, Joint Discussion 7 poster, www.referencesystems.info/presentations-and-posters.html
- Zacharias, M.I. & Zacharias, N. 2013, CDS catalog I/325, Strasbourg
- Zacharias, N. 1996, *PASP* 108, 1135
- Zacharias, N., Zacharias, M.I., Hall, D.M., Johnston, K.J., de Vegt, C., & Winter, L. 1999, *AJ* 118, 2511
- Zacharias, N., 2004, *Proceed. ADeLA2002*, Eds. R.Teixeira, N.V.Leister, V.A.Martin, & P.Benevides-soares, Sao Paulo, p.123
- Zacharias, N., Urban, S.E., Zacharias, M.I., Wycoff, G.L., Hall, D.M., Monet, D.G., & Rafferty, T.J. 2004, *AJ*, 127, 3043
- Zacharias, N. 2010, *AJ* 139, 2208-2217
- Zacharias, N., Finch, C.T., Girard, T.M., Henden, A., Bartlett, J.L., Monet, D.G., Zacharias, M.I. 2013, *AJ* 145, 44

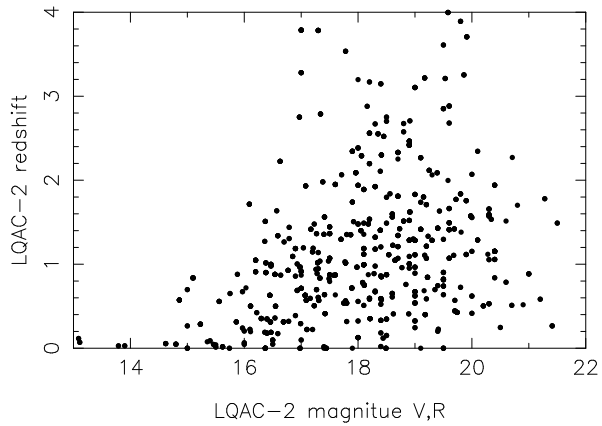


Fig. 1.— Distribution of approximate magnitude (V if available, else R) and redshift of all sources in our investigation. Data are taken from the LQAC-2 catalog.

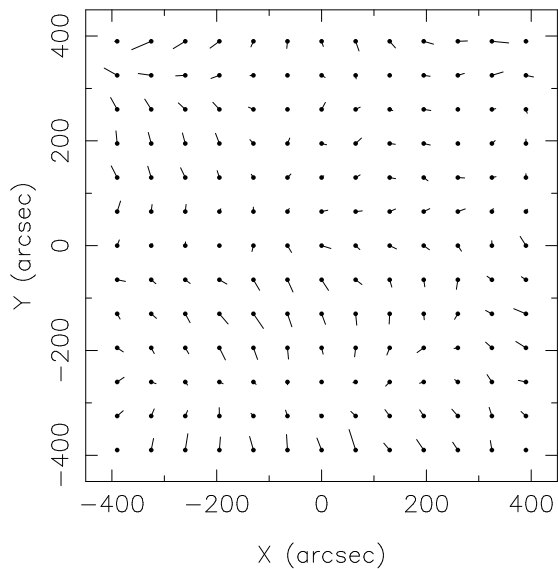


Fig. 2.— Field distortion pattern of the CTIO 0.9 m telescope field of view. Smoothed data are shown from run “q” and UCAC4-type reference star residuals. Vectors are scaled by a factor of 1000.

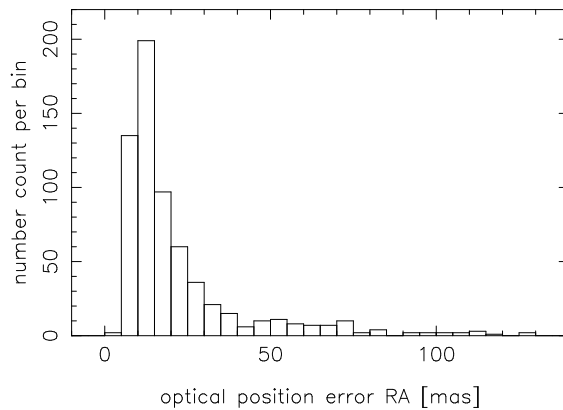


Fig. 3.— Histogram of the total, random, mean optical position errors (per coordinate) from all exposures of an individual source and observing run. These errors include x, y fit errors, contribution from the atmospheric turbulence and error propagation from reference stars.

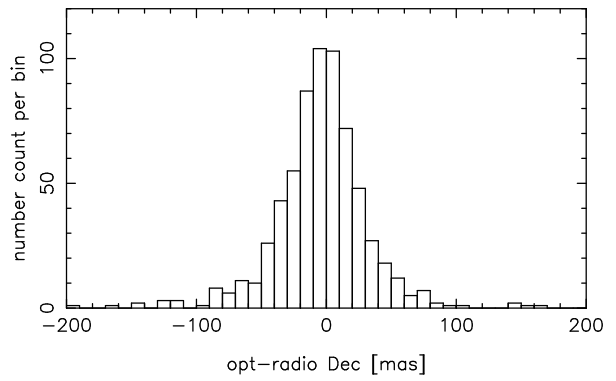
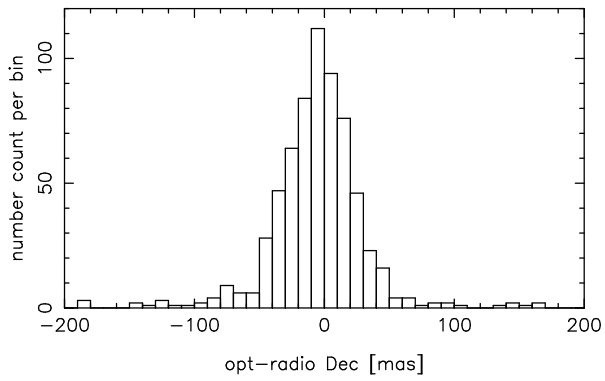
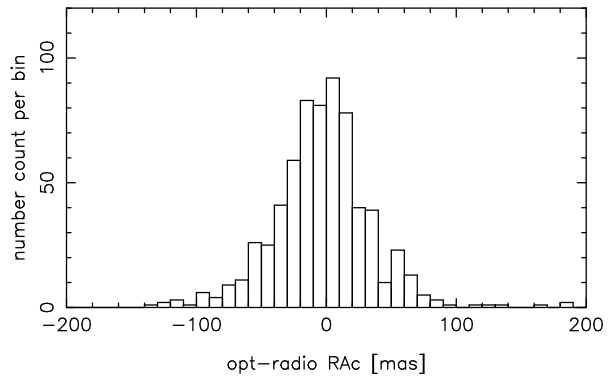
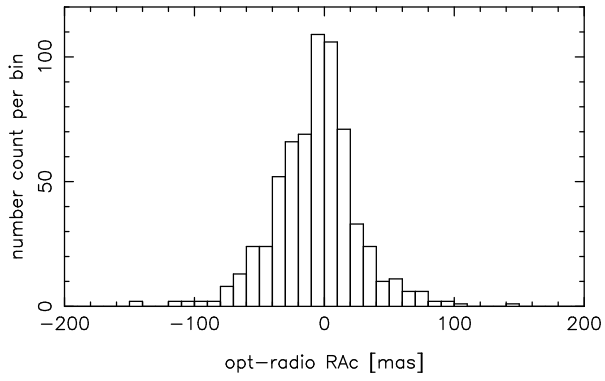


Fig. 4.— Histogram of (optical–radio) position differences per coordinate of our UCAC2-type data.

Fig. 5.— Same as the previous figure but for UCAC4-type data.

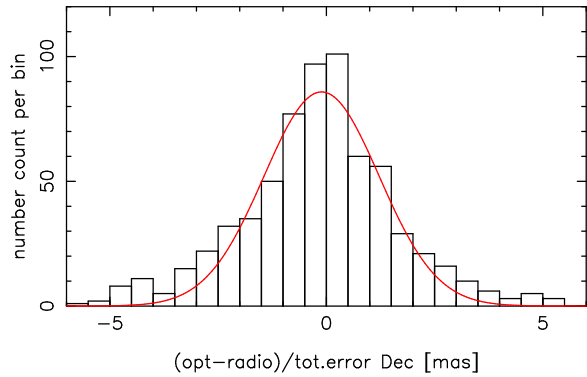
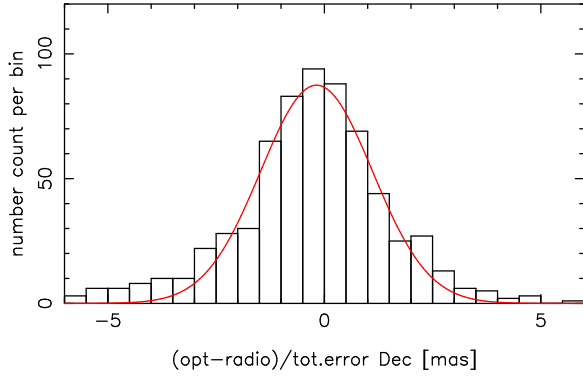
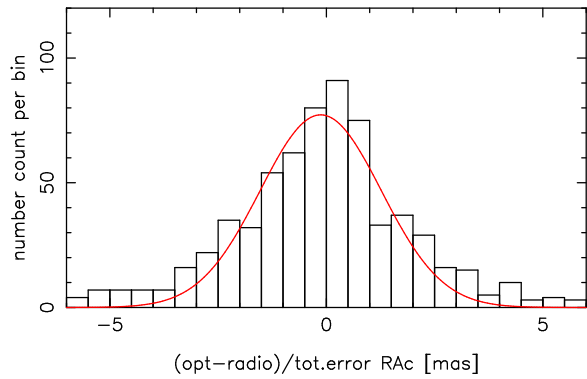
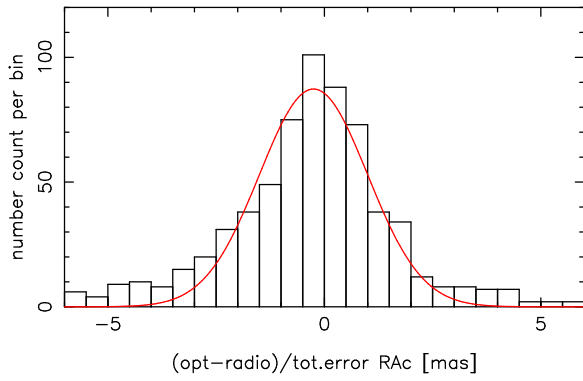


Fig. 6.— Histogram of the scaled $(\text{optical}-\text{radio})/\text{error}$ position differences per coordinate of our UCAC2-type data. The plot line represents the best fit normal distribution.

Fig. 7.— Same as the previous figure but for UCAC4-type data.

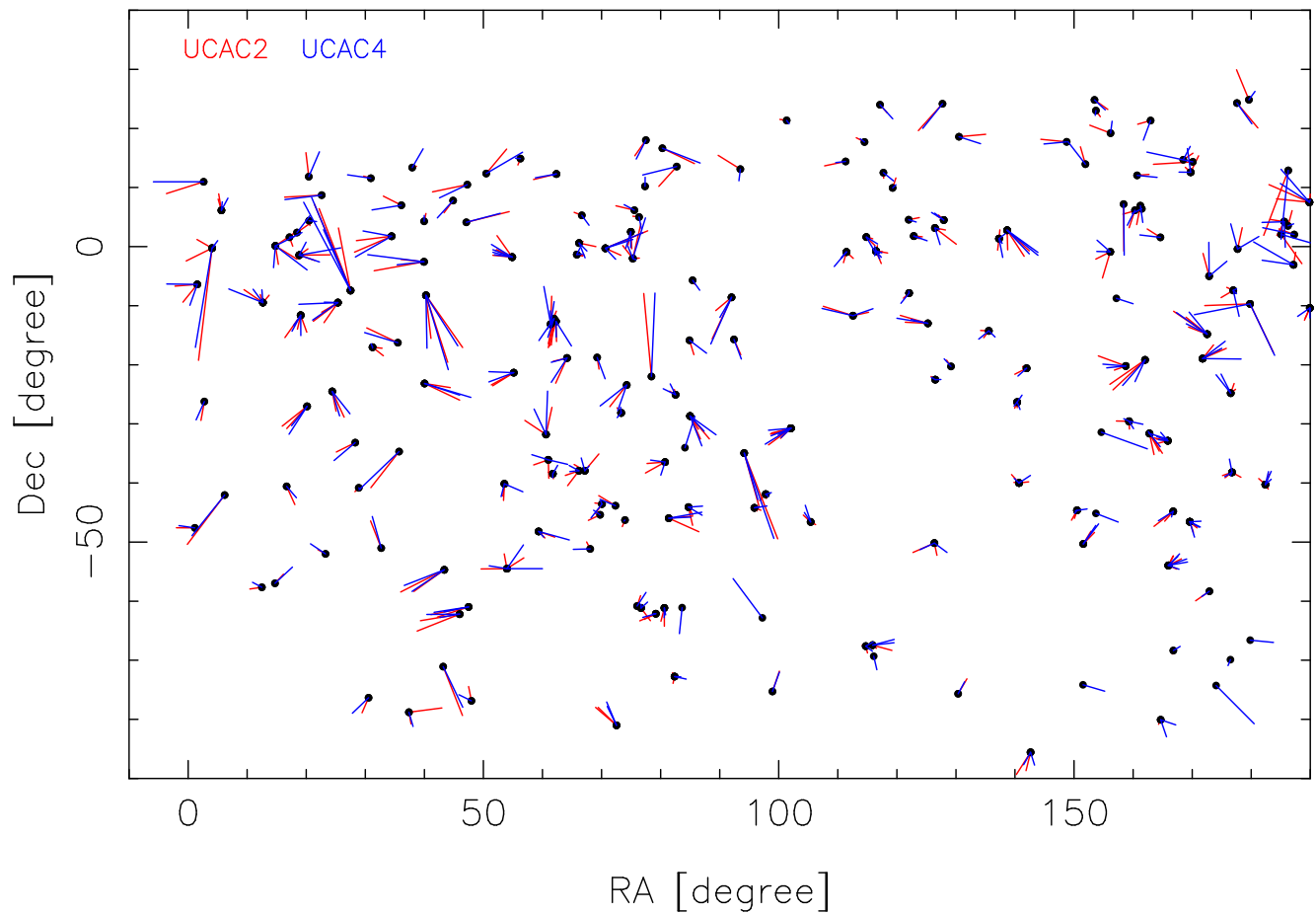


Fig. 8.— Distribution of our sources on the sky with optical–radio position difference vectors shown for each observation. Data from UCAC2 and UCAC4-type processing are shown in red and blue, respectively. The scale of the vectors is 10 mas for 1 degree. Data for 0 th 12 hours RA (0 to 180 deg) are shown here.

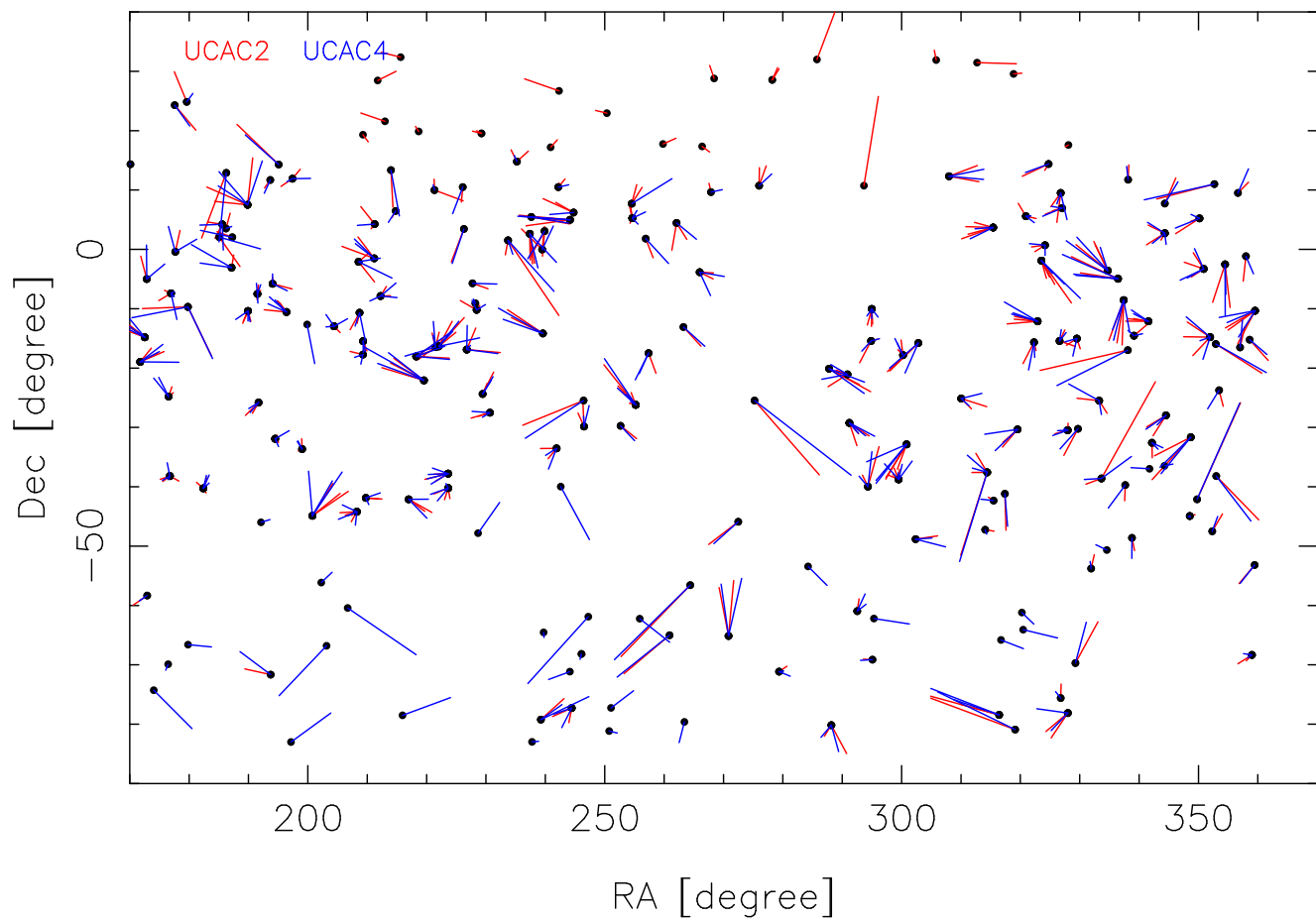


Fig. 9.— The same as the previous figure but for RA = 12 to 24 hours (with some overlap).

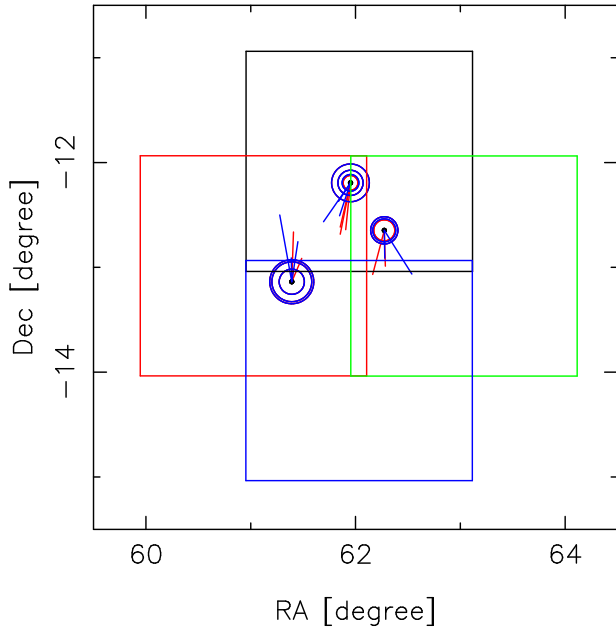


Fig. 10.— A zoom in at the location of the 3 sources 0403–132, 0405–123, and 0406–127 (from left to right) which are at redshifts 0.571, 0.574, and 1.563 respectively. Vectors show optical–radio position differences and circles the 1σ , total, formal errors. The scale of the vectors and circles are 100 mas per 1 degree. Results from multiple observing runs are shown. UCAC2-type data are shown in red, while UCAC4-type data (overwriting UCAC2-type, if same values) are shown in blue. The squares indicate the Astrographic Catalogue plates used to derive the Tycho-2 proper motions.

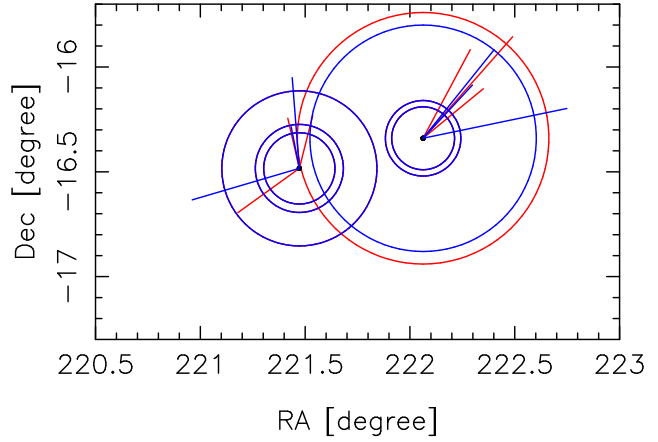


Fig. 11.— Similar to the previous figure, a zoom in at the location of the sources 1443–162 and 1445–161 which are at redshifts unknown and 2.417 respectively.

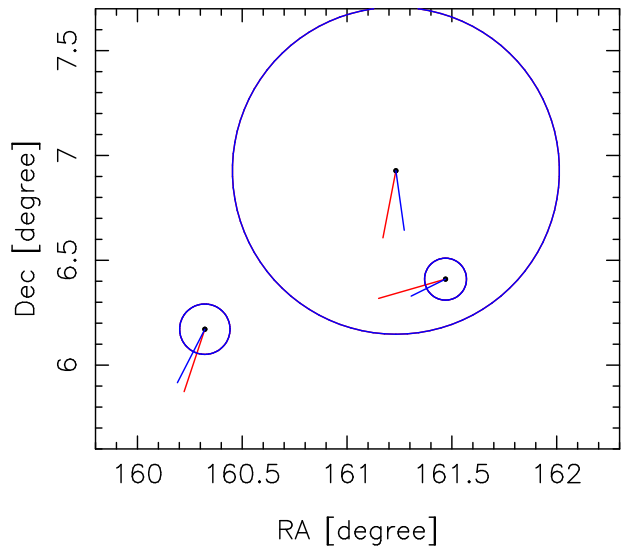


Fig. 12.— Similar to the previous figure, a zoom in at the location of the 3 sources 1038+064, 1042+071, and 1043+066 which are at redshifts 1.265, 0.698, and 1.507 respectively.

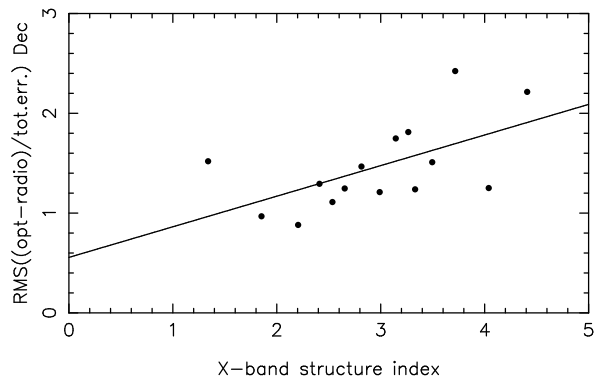
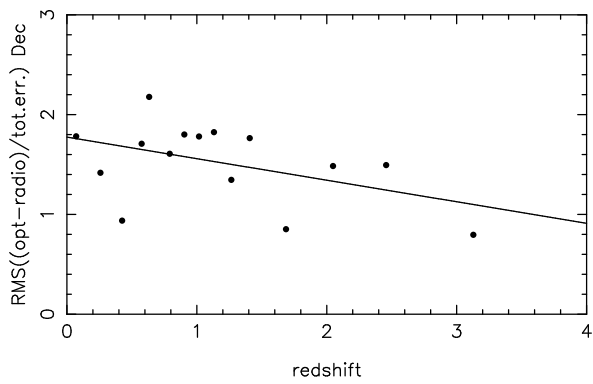
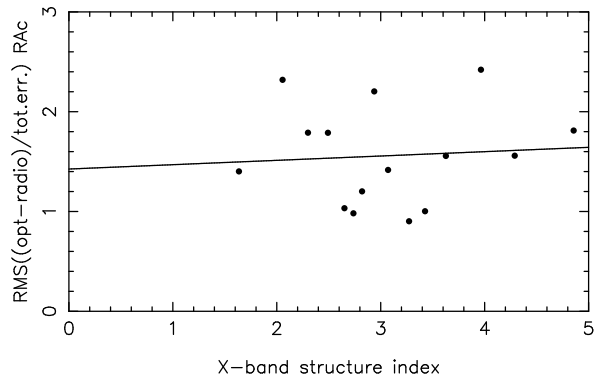
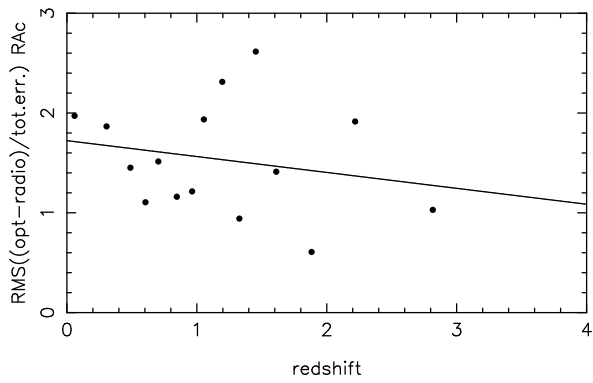


Fig. 13.— Optical–radio position differences over total formal error of individual sources (RMS over 16 offsets per dot) as a function of redshift, RA component on top, Dec at bottom, using UCAC2-based results.

Fig. 14.— Same as previous figure but as a function of X-band radio structure index.

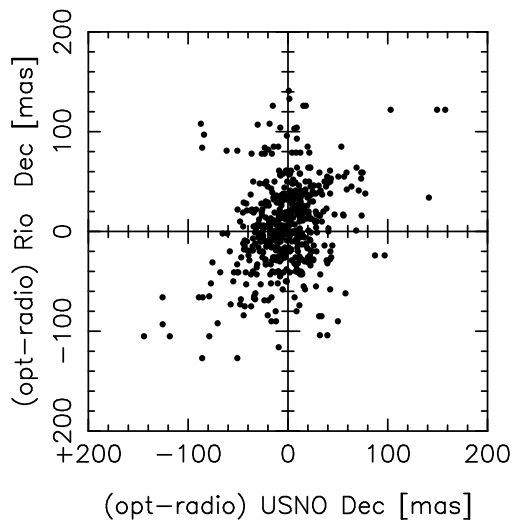
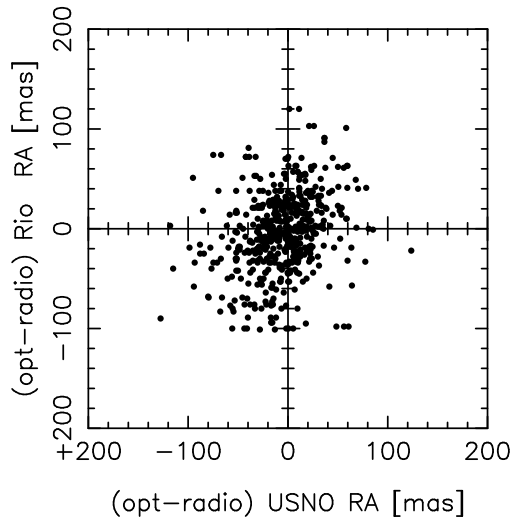


Fig. 15.— Comparison of optical–radio position differences of individual source observations of our investigation versus the Rio survey data of the 281 sources in common. The top figure shows the result for the RA component, the bottom for Dec.

Table 1: Overview of deep CCD imaging observing runs used for this investigation. Each run is identified with a letter. The telescope used is identified and the observing epoch is given. The last 3 columns give the number of observing nights, total number of ICRF source fields observed (including partial data and empty fields), and the initials of the observers (see acknowledgment).

ID	telescope	date	n	s	obs
o	CTIO 0.9 m	Dec 1997	5	37	MZ, NZ
p	CTIO 0.9 m	Feb 1998	5	29	MZ, NZ
q	CTIO 0.9 m	Jul 1998	6	46	MZ, NZ
r	CTIO 0.9 m	Aug 1998	6	44	MZ, NZ
s	CTIO 0.9 m	Jan 1999	5	56	NZ, TR
t	CTIO 0.9 m	Mar 1999	5	56	MZ, NZ, JP
u	CTIO 0.9 m	Jun 1999	4	61	MZ, NZ
v	CTIO 0.9 m	Sep 1999	6	52	TR
w	CTIO 0.9 m	Dec 1999	5	57	NZ
x	CTIO 0.9 m	Mar 2000	4	77	TR
y	CTIO 0.9 m	Jun 2000	5	51	NZ
z	CTIO 0.9 m	Sep 2000	5	77	TR
a	CTIO 0.9 m	Jan 2001	5	39	EH
b	KPNO 2.1 m	Jun 2001	5	42	MZ
J	CTIO 0.9 m	May 2004	5	66	NZ

Table 3: The USNO “redlens” astrograph and camera used for the secondary reference star observations.

item	description
clear aperture	206 mm
focal length	2057 mm
number of lens elements	5
corrected for bandpass	550–710 nm
diameter usable field of view	≈ 9 degree
active guiding with	ST4 at visual lens
number of pixels	4095 x 4095
field of view	61 x 61 arcmin
pixel size	9.0 μm
pixel scale	0.905 arcsec/pixel
spectral bandpass used	579–642 nm
limiting magnitude	≈ 16.0 2 min.

Table 2: Observing of ICRF source fields at the astrograph.

item	description
observing dates	Jan 1998 to June 2003
number of frames total	14,653
number of frames rejected	about 20 %
exposure times	30 and 150 sec
typical number of frames	
per run and source	8 – 16
control of system.errors	observe on both sides of pier
plus observe	calibration fields frequently
astrograph imaging	within 2 weeks of deep runs

Table 4: Results from UCAC2-type reductions of ICRF optical counterparts. For a detailed explanation of columns see text. Only example lines are shown here, the complete table with 666 lines is available as catalog I/325 from CDS.

1			2			3			4			5		6		7		8		9		10		11		12		13		14		15	
RAJ2000			DEJ2000			RAJ2000			DEJ2000S			dRAc	dDec	dist	eRA	eDE	sRA	sDE	eRad	Nccd	Nr	Nrx											
h	m	s	d	'	"	degree	degree	mas	mas	mas	mas	mas	mas	mas	mas	mas	mas	mas	mas	mas	mas	mas	mas	mas	mas	mas	mas	mas	mas	mas	mas	mas	
00	04	35.6524	-47	36	19.603	0.07657011	-47.6054454	31.4	-31.4	0.3	13.	13.	-2.4	0.0	0.2	5	20	1															
00	06	13.8912	-06	23	35.366	0.10385868	-6.3931571	38.9	-24.5	-30.2	29.	29.	-0.8	-1.0	0.0	3	18	0															
00	06	13.8903	-06	23	35.338	0.10385843	-6.3931495	38.0	-37.9	-2.9	12.	12.	-3.2	-0.2	0.0	4	20	0															
00	10	31.0016	+10	58	29.484	0.17527823	10.9748568	66.0	-62.9	-19.9	13.	13.	-4.8	-1.5	0.1	4	15	3															
00	11	01.2463	-26	12	33.409	0.18367953	-26.2092803	32.6	-5.8	-32.1	62.	62.	-0.1	-0.5	0.1	1	16	0															
00	16	11.0870	-00	15	12.635	0.26974640	-0.2535098	191.3	-22.7	-189.9	116.	116.	-0.2	-1.6	0.1	4	17	1															
00	16	11.0856	-00	15	12.467	0.26974601	-0.2534631	48.9	-43.8	-21.8	67.	67.	-0.7	-0.3	0.1	4	15	1															
00	16	11.0869	-00	15	12.431	0.26974635	-0.2534530	29.2	-25.4	14.5	44.	44.	-0.6	0.3	0.1	3	20	0															
00	22	32.4409	+06	08	04.297	0.37567803	6.1345269	28.2	-4.5	27.8	37.	37.	-0.1	0.8	0.1	4	21	1															
00	22	32.4408	+06	08	04.288	0.37567801	6.1345245	28.2	-4.5	27.8	37.	37.	-0.1	0.8	0.1	4	21	1															
00	24	42.9841	-42	02	04.032	0.41194003	-42.0344532	88.2	-55.2	-68.8	74.	74.	-0.9	-1.1	1.3	2	19	0															

Table 5: Explanation of optical source quality flag (column 24 of Tables 4 and 5).

flag	description
g	good optical source
f	faint optical source ($S/N \leq 5$)
u	unconfirmed, too faint for unique ID
l	large (opt.-radio) pos.diff. ($\geq 3\sigma$)
p	problem case, ($\geq 5\sigma$) or blended image
n	not an ICRF source

Table 5: Results from UCAC4-type reductions of ICRF optical counterparts. For a detailed explanation of columns see text. Only example lines are shown here, the complete table with 682 lines is available as catalog I/325 from CDS.

1			2			3			4			5		6		7		8		9		10		11		12		13		14		15	
RAJ2000			DEJ2000			RAJ2000			DEJ2000S			dRAc	dDec	dist	eRA	eDE	sRA	sDE	eRad	Nccd	Nr	Nrx											
h	m	s	d	'	"	degree	degree	mas	mas	mas	mas	mas	mas	mas	mas	mas	mas	mas	mas	mas	mas	mas	mas	mas	mas	mas	mas	mas	mas	mas	mas		
00	04	35.6528	-47	36	19.600	0.07657023	-47.6054444	27.4	-27.1	3.9	19.	19.	-1.4	0.2	0.2	2	20	0															
00	06	13.8920	-06	23	35.371	0.10385890	-6.3931585	37.5	-12.6	-35.3	29.	29.	-0.4	-1.2	0.0	3	21	0															
00	06	13.8894	-06	23	35.335	0.10385817	-6.3931485	51.8	-51.8	0.7	12.	12.	-4.3	0.1	0.0	4	26	0															
00	10	31.0001	+10	58	29.504	0.17527781	10.9748623	85.2	-85.2	-0.1	12.	12.	-7.1	0.0	0.1	4	29	0															
00	11	01.2457	-26	12	33.408	0.18367936	-26.2092800	34.0	-14.0	-31.0	62.	62.	-0.2	-0.5	0.1	1	17	0															
00	16	11.0867	-00	15	12.613	0.26974630	-0.2535037	170.3	-28.1	-168.0	116.	116.	-0.2	-1.4	0.1	4	23	0															
00	16	11.0889	-00	15	12.441	0.26974691	-0.2534558	6.6	4.8	4.5	67.	67.	0.1	0.1	0.1	4	16	0															
00	16	11.0892	-00	15	12.433	0.26974700	-0.2534535	16.0	9.7	12.7	44.	44.	0.2	0.3	0.1	3	25	0															
00	22	32.4413	+06	08	04.284	0.37567814	6.1345232	14.5	1.4	14.4	37.	37.	0.0	0.4	0.1	4	20	0															
00	22	32.4420	+06	08	04.290	0.37567832	6.1345249	23.4	11.1	20.6	19.	19.	0.6	1.1	0.1	4	22	0															
00	24	42.9848	-42	02	04.017	0.41194023	-42.0344491	88.2	-55.2	-68.8	74.	74.	-0.7	-0.9	1.3	2	19	0															

Table 7: List of empty fields. These are ICRF sources where no optical counterpart could be detected at the radio position. Column 1 gives the ICRF source name, column 2 lists the observing runs in which the field was observed (see Tab. 1), column 3 gives the total number of deep exposures, and the last column adds comments, if available. For some cases offset coordinates between an object visible on the deep CCD exposures and the ICRF radio position is given in arcsec for the RA and Dec component, respectively, in the comment column.

source	runs	n.exp.	comment
0008-421	r	2	
0201+088	z	1	
0334+014	w	6	-21.6 -2.5 off bright star
0615-365	t	2	
0637-337	t	2	
0647-475	p,t	4	high uncertainty radio position
0733-174	J	5	
0736-332	s	2	
0826-373	p,s,t,w,o	31	offset = 2.3 5.5, calibr.field
0831-445	s,t	13	offset = -2.3 0.8, VELA-G
0833-450	p,s,t	16	offset: 5.0 0.1
0903-573	J	4	
1039-474	p,s	8	high uncertainty radio position
1148-671	p	5	offset = 0.6 5.0, crowded field
1234-504	J	3	
1236-684	p	2	offset = -2.7 3.6
1251-407	p,s	5	
1334-649	r	5	offset = -0.9 -3.4
1352-632	q	5	offset = -3.9 -4.3, crowded field
1420-679	J	7	
1448-648	J	4	
1508-656	r	4	
1600-445	q	8	offset = -1.7 1.3, crowded field
1740-517	q	5	offset = 0.0 -8.3
1822-173	J	4	star within 1 arcsec
1829-106	J	6	
1829-718	q,r	5	offset = 2.5 -1.8
1929+226	b	13	offset = 1.9
1932+204	b	2	
1943+228	b	7	offset = 3.0, crd field
1950-613	J	3	
2008-068	y,z	4	
2128+048	y	2	
2259-375	q	1	
2300-307	q,v	8	offset = 1.1 -3.8, inside halo of bright star
2333-528	r	5	offset = 2.1 8.2

Table 8: Eulerian orientation angles (w1,w2,w3) between optical and radio coordinate system from various least-squares solutions of Table 4 and 5 data. Consecutive lines show results from 2 models (with and without declination offset term). Results from weighted (w) and unweighted (u) solutions as well as with different restrictions (see text) are shown. See text for more explanations.

sigma mas	ndf	w1 mas	w2 mas	w3 mas	dcoeff mas	errors mas mas mas mas				notes of solution
26.75	1240	4.93	-4.78	7.61		1.42	1.34	1.21		u,2, 3sig
26.55	1239	4.55	-5.11	7.78	-5.14	1.42	1.32	1.20	1.07	
17.94	1195	6.59	-3.84	6.96		0.98	0.92	0.87		w,2, 3sig
17.94	1197	6.13	-4.51	6.88	-3.58	0.98	0.93	0.87	0.76	
28.98	1261	5.48	-4.71	7.46		1.53	1.44	1.30		u,2, 4sig
28.58	1259	5.36	-5.06	7.47	-5.31	1.51	1.42	1.28	1.14	
23.24	1272	3.44	-3.85	7.39		1.20	1.15	1.06		w,2, 4sig
22.85	1270	3.50	-4.72	7.43	-5.05	1.18	1.14	1.04	0.91	
29.71	1263	5.10	-3.89	3.92		1.56	1.44	1.37		u,4, 3sig
29.81	1264	4.60	-3.71	3.92	-3.60	1.56	1.44	1.37	1.19	
18.44	1184	5.82	-3.33	3.06		1.02	0.95	0.94		w,4, 3sig
18.45	1185	4.51	-4.22	2.93	-2.84	1.02	0.97	0.94	0.79	
33.06	1291	4.15	-4.00	5.50		1.71	1.58	1.50		u,4, 4sig
32.93	1290	3.83	-4.20	5.50	-4.34	1.71	1.58	1.50	1.30	
24.63	1287	4.62	-5.70	5.23		1.27	1.19	1.13		w,4, 4sig
24.65	1287	4.68	-6.19	5.21	-3.15	1.27	1.20	1.13	0.99	

Table 10: List of nearest neighbor sources in our sample.

separation (degree)	ICRF name		optical–radio source 1, 2				pos.error		Fig. numb.
	source1	source2	RA (mas)	Dec (mas)	RA (mas)	Dec (mas)	src.1 (mas)	src.2 (mas)	
0.556	0405–123	0406–127	-9	-45	-5	-38	12	12	10
0.569	1042+071	1043+066	-6	-32	-32	-9	78	10	
0.608	1443–162	1445–161	-6	+24	+22	+42	17	15	11
0.752	0503–608	0506–612	+6	+18	+9	-12	59	10	
0.943	1219+044	1222+037	-18	-10	+7	+26	10	28	
0.977	0457+024	0500+019	+2	-28	+92	-313	15	250	
0.992	0422–380	0426–380	-20	-25	-18	+11	11	17	
1.009	0403–132	0406–127	+6	+20	-5	-38	12	12	10
1.123	1510–089	1511–100	-2	+4	-11	+11	12	11	
1.157	0738–674	0743–673	+2	-8	+7	-5	12	6	
1.173	1038+064	1043+066	-10	-30	-32	-9	12	10	12